1,3 dipolar cycloaddition of münchnones: Factors behind the regio-selectivity

Meylin Bocalandro,[†] Juan J. González Armesto,[‡] Luis A. Montero-Cabrera,[†] and Marco Martínez González[*,†]

†*Laboratory of Computational and Theoretical Chemistry, Faculty of Chemistry, University of Havana, Havana, Cuba*

‡*Department of Applied Physics, Physics Faculty, University of Havana, Cuba*

E-mail: mmg870630@gmail.com

Abstract

The 1,3 dipolar cycloaddition reactions of münchnones and alkenes provide an expedite synthetic way to substituted pyrroles, an exceedingly important structural motif in the pharmaceutical and material science fields of research. The factors governing their regio-selectivity rationalization are not well understood. Using several approaches, we investigate a set of 14 reactions (featuring two münchnones, 12 different alkenes, and two alkynes). The Natural Bond Theory and the Non-Covalent Interaction Index analyses of the non-covalent interaction energies fail to predict the experimental major regio-isomer. Employing global cDFT descriptors or local ones such as the Fukui function and dual descriptor yields similarly inaccurate predictions. Only the local softness pairing, withing Pearson's Hard and Soft Acids and Bases principle, constitutes a reliable predictor for the major reaction product. By taking into account an estimator for the steric effects, the correct regio-isomer is predicted. Steric effects play a major role in driving the regio-selectivity, as was corroborated by energy decomposition analysis of the transition states.

Introduction

N-containing heterocycles are ubiquitous in nature. These structural motifs are present in many bio-molecules, such as DNA basis, hormones, and proteins, participating in multiple key metabolic processes.[1,2] At the same time, they show intrinsic reactivity[3,4], being able to partake in numerous highly efficient reactions, which opens the door to synthetic ways to modify their chemical and physical properties. It comes then as no surprise their paramount relevance for the pharmaceutical and material design fields of research. For example, more than half of the FDA-approved small molecules feature at least one N substituted heterocycle (59% up to 2014[5,6] and 88% from 2015 to 2020[7]).

In particular, the pyrrole structural motif and its derivatives are present in many natural and man-made products and molecules with pharmaceutical properties[8], such as antibiotics[9–11], anti-inflammatory drugs[12,13], anticancer drugs[14–16], and HIV drug candidates[17–19] among others. Therefore, finding novel efficient synthetic routes for pyrrole derivatives acquires special relevance. A promising new alternative for their obtention is the 1,3 dipolar cycloaddition (13DC) of münchnones (1,3-oxazolium 5-oxides)[20–22]. These reactions produce bicyclic cycloadducts which can undergo CO_2 loss under simple conditions yielding substituted pyrroles. At the same time, they classify within the *click chemistry* philosophy[23,24], as they proceed under simple reaction conditions and are characterized by their high yield and carbon efficiency. The reactions also present high regio-selectivity, even in the absence of catalyzers. Consequently, it is not surprising the large number of theoretical and experimental works devoted to studying them[22,25–28].

The regio-selectivity of 13DC of münchnones and phosphomünchnones with alkynes was intensely explored in a series of theoretical works by Houk et al.[29–31] For these reactions, the frontier molecular orbital theory (FMO) failed to correctly predict the major product from their reactants[29]. Only by employing a distortion interaction analysis, they were able to rationalize the reactivity of such systems, finding the molecular distortion effects being the major driving factor behind the regio-selectivity. A posterior research, focused on 13DC

of alkenes with münchnones, was undertaken by Lopchuk et al.[32] by means of experimental determinations and theoretical calculations. In particular, they studied the reaction of two münchnones with several phenyl-substituted nitro alkenes, and with phenylacetylene. For these cases, FMO failed to predict the major product. A hypothesis was then made that steric effects were driving the reaction selectivity. Nevertheless, the insensibility of the major regio-isomer to changes in the bulkier group position in the münchnone ring results very intriguing.

A recent investigation was performed[33] using conceptual density functional theory[34] (cDFT) tools along the reaction path for a representative reaction of this family. All tested descriptors failed to predict the experimental regio-selectivity of the reaction, and the greatest charge transfer (which is when cDFT descriptors were devised to be more accurate) materializes after the transition state (TS). It was also noted that although the 13DC occurs in one elementary step, bond formation between dipole and dipolarophile occurs asynchronously.

This work extends the previous research[33] to a bigger subset of the reactions compiled by Lopchuk et al.[32] aiming to understand the main factors driving the reaction's regio-selectivity. Initially, we locate the most important dipole-dipolarophile interactions in the TSs, assessing their relevance to the regio-selectivity. For this, we perform a thorough analysis of the TSs' electronic density within the natural bond orbital[35–37] (NBO) and non-covalent interaction index[38,39] (NCI) frameworks. Several global and local conceptual density functional theory (cDFT) descriptors[34,40] combined with different condensation[40–43] (to numerical values) schemes were later used to rationalize the regio-selectivity. Also, directional analysis of the münchnones steric repulsion[44,45] effects on the regio-selectivity was performed, followed by an assessment of its relevance by means of an energy decomposition analysis (EDA)[46–48].

Conceptual Density Functional theory

During the course of a reaction, when two reactants approach and interact, each one of them is perturbed by the other. The external potential acting on the electrons of each molecule changes (from $v(r)$ to $v(r)+\Delta v(r)$) due to the additional interaction with the other reactant's nuclei and electrons. At the same time, as charge transfer processes occur, the total number of electrons (of each molecule) is also affected (it changes from N to $N+\Delta N$). The energy variation associated with the interaction can be expressed as a Taylor series in terms of ΔN and $\Delta v(r)$[40,49,50]:

$$\Delta E = E[v(r)+\Delta v(r); N+\Delta N] - E[v(r); N] \tag{1}$$

$$= \left(\frac{\partial E}{\partial N}\right)_{v(r)} \Delta N + \int \left(\frac{\delta E}{\delta v(r)}\right)_N \Delta v(r) dr + \frac{1}{2}\left(\frac{\partial^2 E}{\partial N^2}\right)_{v(r)} \Delta N^2 + \int \left(\frac{\delta^2 E}{\delta v(r)\partial N}\right)_N \Delta N \Delta v(r) dr + \frac{1}{2}\int \left(\frac{\delta^2 E}{\delta v(r)\delta v'(r)}\right)_N \delta v'(r)\delta v(r) dr dr' + \ldots \tag{2}$$

In favorable interactions, the system stabilizes and energy decreases, with the differentials of energy (or energy response functions) in equation 2 providing information about the system's reactivity. In conceptual density functional theory (cDFT), these response functions are linked to chemical concepts widely employed to qualitatively rationalize and predict the reactivity of molecular systems[40,51].

The position-independent (r) partial derivatives in equation 2 are called global descriptors. Global descriptors measure the overall response of a system to different kind of attacks (nucleophilic/electrophilic) and have been linked to concepts, such as chemical potential $\mu = \left(\frac{\partial E}{\partial N}\right)_{v(r)}$, electronegativity[52,53] $\chi = -\mu$, chemical hardness[54] $\eta = \left(\frac{\partial^2 E}{\partial N^2}\right)_{v(r)}$, chemical softness[40,55] $S = \frac{1}{\eta}$, and electrophilicity[56–58] $\omega = \frac{\mu^2}{2\eta}$. Typically, μ and η, from which the other

global descriptors can be derived, are calculated from the following working approximations:

$$\mu = \frac{I + A}{2} \tag{3}$$

$$\eta = I - A \tag{4}$$

where I and A are the vertical ionization potential $I = E(N-1) - E(N)$ and electron affinity $A = E(N) - E(N+1)$ of the system[55].

As the reaction evolves, charge transfer is expected from the less electronegative (lower χ value) reagent to the other. A simple comparison of the calculated electronegativity values yields a prediction of the (donor/acceptor) character for each of the species involved in the reaction.

Global descriptors can also provide information on a reaction's regio-selectivity. Several derived "reactivity principles" have been employed to predict the preferred product/TS among possible alternatives. In this work, we assessed the capabilities of three cDFT principles to predict a reaction's major product:

$\Delta|\mu|$ **big is good:** [59–61] A reaction will evolve preferably in the direction that maximizes the variation of the chemical potential. That is to say, the favored product (or TS) is the one involving the biggest electronegativity change $|\Delta\mu|$ with respect to the reactants, where $|\Delta\mu| = |\mu_x - (\mu_a + \mu_b)/2|$ with x standing for the TS and a, b for the reactants.

Máximun hardness η: [62,63] A reaction will evolve preferably to the configuration (TS/product) for which the hardness is maximized.

Minimum electrophilicity ω: [64,65] Molecules tend to decrease their electrophilicity during a reaction. Given a set of possible reaction outcomes, the preferred TS/product is the one with the lowest electrophilicity (ω).

Another group of cDFT descriptors are associated to the response functions in equation 2 presenting an explicit dependence on r. These are known as local descriptors and encode

information about the system's local susceptibilities to gain/lose electron density[50,55]. Consequently, they act as natural markers for the regio-selectivity of reactive processes. Two of the most widely employed local descriptors regarding regio-selectivity studies are:

The Fukui function: [66–69]

$$f(r) = \left(\frac{\delta^2 E}{\delta v(r)\delta N}\right) = \left(\frac{\delta \mu}{\delta v(r)}\right)_N = \left(\frac{\partial \rho(r)}{\partial N}\right)_{v(r)} \tag{5}$$

describing the electronic density's response to variations of the molecule's number of electrons.

The dual descriptor: [70–73]

$$\Delta f(r) = \left(\frac{\delta^3 E}{\delta v(r)\partial^2 N}\right) = \left(\frac{\partial f(r)}{\partial N}\right)_{v(r)} = \left(\frac{\delta \eta}{\delta v(r)}\right)_N \tag{6}$$

For molecular systems, the energy's derivative with respect to the number of particles is discontinuous. Because of this, to obtain working approximations for $f(r)$ and $\Delta f(r)$ it is necessary[74–76] to define the one-sided derivatives. Within the finite differences method (FD) the derivatives take the form:

$$f^+(r) = {}^{N+1}\rho(r) - {}^{N}\rho(r) \tag{7}$$

$$f^-(r) = {}^{N}\rho(r) - {}^{N-1}\rho(r) \tag{8}$$

Another approximation, using spin densities, was proposed by Galván, Gázquez, and Vela (GGV)[77]:

$$f^+(r) = {}^{N+1}\rho_s(r)/{}^{N+1}N_s \tag{9}$$

$$f^-(r) = {}^{N-1}\rho_s(r)/{}^{N-1}N_s \tag{10}$$

Here, ${}^{M}\rho(r)_s = {}^{M}\rho_\alpha(r) - {}^{M}\rho_\beta(r)$ are spin densities, and, ${}^{M}N_s = {}^{M}N_\alpha - {}^{M}N_\beta$ spin numbers.

$f^+(r)$ and $f^-(r)$ provide local measures for the propensities to experience nucleophilic or electrophilic attacks. If a molecule acts as an electron acceptor, the electrons go towards the region with the greatest $f^+(r)$. Correspondingly, when it acts as electron donor, the electrons will part from the region with the greatest $f^-(r)$ values. The regions with greater $f^+(r)$ and $f^-(r)$ mark the zones of the molecule displaying a more pronounced electrophilic and nucleophilic characters, respectively.

Using the FD method, with $f^+(r)$ and $f^-(r)$, is possible to compute the dual descriptor $\Delta f(r)$:

$$\Delta f(r) \cong f^+(r) - f^-(r) \tag{11}$$

comprising information about both the nucleophilic/electrophilic character of a molecule. Regions prone to accept electrons will display $\Delta f(r) > 0$ while zones prone to lose electrons will show $\Delta f(r) < 0$. When the reactants approach, regions with $\Delta f(r) < 0$ (donor character) of a molecule will bond to regions with $\Delta f(r) > 0$ (acceptor character) from the other. This insight allows us to perform regio-selectivity and even stereo-selectivity predictions, even for reactive processes where each reactant gain and lose electron density simultaneously.

A strictly visual analysis of $f(r)$ and $\Delta f(r)$ results' can prove complex. In situations where two or more reactive sites share the same character, the more "nucleophilic/electrophilic" atom can be estimated by the size of the corresponding lobes. Nevertheless, this approach can be prone to errors due to the subjective nature of the visual inspection. Also, the visual analysis turns difficult when the same atom presents lobes representing both characters (in the case of $\Delta f(r)$), as often occurs for FD-generated isosurfaces. A viable alternative relies on condensing the descriptors in atomic domains, resulting in numeric values that simplify the process of assessing the relative character of the involved atoms. The condensed expressions

for $f(r)$ are:

$$f_k^+ = {}^N q_k - {}^{N+1} q_k \tag{12}$$

$$f_k^- = {}^{N-1} q_k - {}^N q_k \tag{13}$$

where q corresponds to the natural atomic charge and the index k identifies the atom. Substituting 12 and 13 in equation 11 leads to the atomically condensed dual descriptor values:

$$\Delta f_k = 2^N q_k - {}^{N-1} q_k - {}^{N+1} q_k \tag{14}$$

Although atomically condensed local descriptors conduce to numeric results, making easier the comparisons, it is important to point out the intrinsic arbitrariness in the selection of a partition scheme of the molecular system into atomic domains. Another issue lies in considering (or not) the variation of the atoms domain frontiers with the exchange of electrons. Simultaneously, since the descriptors are integrated over the atomic domains, an inherent limitation lies in the loss of information about the geometrical orientation of $f(r)$ and $\Delta f(r)$. This becomes especially problematic for $\Delta f(r)$ in atoms that exhibit, depending on the direction, both donor or acceptor character lobes. In these cases, the (donor/acceptor) atom character should be determined by the lobe of $\Delta f(r)$ with the correct geometrical orientation, not the total integral. Aiming to reduce the possibility of ending with an incorrect prediction Tognetti et al.[42] have developed an efficient algorithm to partition the space into regions occupied by each dual descriptor lobe for a given isosurface value. Following Tognetti's partition, the $\Delta f(r)$ values can be integrated within the domains, providing easily comparable condensed values for the lobes responsible for the reactivity.

An alternative way to predict the regio-selectivity within the cDFT framework is following the matching criteria provided by the local version of Pearson's[78] Hard and Soft Acids and Bases (HSAB) principle[79–81]. The core idea is that atoms with a higher propensity to react will be the ones with more similar softness/hardness.

The local softness is defined as:

$$s(r) = \left(\frac{\partial \rho(r)}{\partial \mu}\right)_{v(r)} \tag{15}$$

or rewriting the expression:

$$s(r) = \left(\frac{\partial \rho(r)}{\partial N}\right)_{v(r)} \times \left(\frac{\partial N}{\partial \mu}\right)_{v(r)} = f(r)S \tag{16}$$

It becomes apparent that $s(r)$ will inherit the discontinuities of $f(r)$ resulting in different values when gaining ($s^+(r)$) or losing ($s^-(r)$) electrons[33,55].

$$s^+(r) = f^+(r) \cdot S \tag{17}$$

$$s^-(r) = f^-(r) \cdot S \tag{18}$$

The atomically condensed values for s_k^+ and s_k^- can be obtained substituting in equations 17 and 18, the condensed f_k^+ and f_k^- values (equations 12 and 13).

$$s_k^+ = f_k^+ \cdot S \tag{19}$$

$$s_k^- = f_k^- \cdot S \tag{20}$$

The most favored interaction will be for the atom pair X,Y (X from the donor and Y from the acceptor of electronic density) that minimizes the norm $d(s_x^-, s_y^+) = (s_x^- - s_y^+)^2$ of difference between the local softness values.

Computational methods

The systems selected for this study were the 13DC reactions of two münchnones, denoted A and B (Figure 1) with seven dipolarophiles, labeled as 3-8, 14 (Figure 2). The relation of

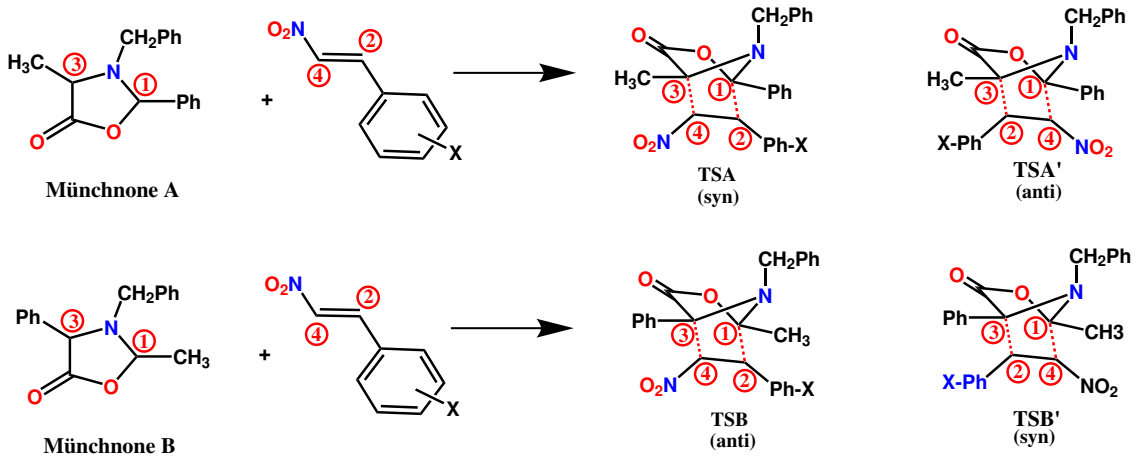

Figure 1: Reactions studied in the present study. The reactive atoms are labeled 1 to 4 for easy reference.

the major (syn/anti) experimental product according to the work of Lopchuk et al[32] can be found in Table 1.

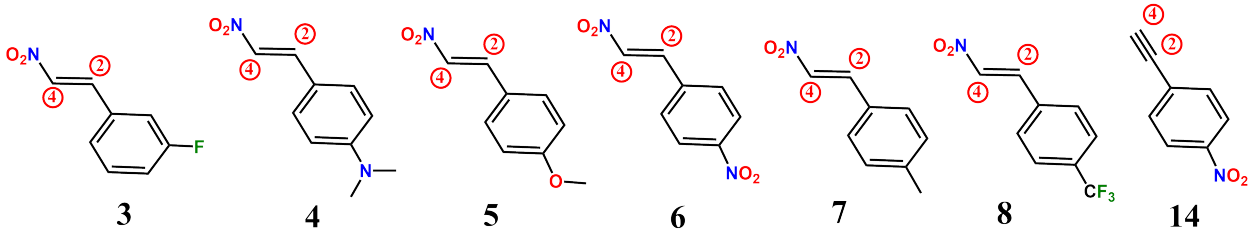

Figure 2: Reactions dipolarophiles corresponding to the studied reactions. The most important reactive C atoms are labeled.

All calculations included in the present work were performed using the B3LYP/6–311G** level of theory as implemented in the Gaussian 09 software[82]. During the reaction, a bond formation process is taking place. These processes usually cannot be well described using single reference methods, and thus although the multiplicity of the total system is singlet, all calculations were performed using the unrestricted approach.

The geometry of the reactants, and the corresponding TSs (both, the ones producing the major and the minor products), were optimized for all reactions. Frequency calculations were performed in each case, to verify there were no imaginary frequencies corresponding to the reactant's geometries and only one imaginary frequency for each TS geometry. Intrinsic

reaction path calculations (IRC) were employed for each TS to verify it successfully connected the reactants to the cycloadducts.

Single-point calculations were done for all species with a positive and a negative charge (at the same geometry) to obtain the vertical ionization energies and electron affinities. The natural bonding orbital (NBO)[35,37,43] and non-covalent interaction[38,39] (NCI) schemes were employed to perform the electronic density analysis of all TSs. Natural charges[43] were used to assess the charge transfer processes in the TSs and to obtain the atomically condensed local descriptors. This approach takes into account the expansion/contraction of the atomic domains in the presence of charge transfer processes.

To characterize the influence of the steric effects on the regio-selectivity, the magnitude of steric force[45] was computed along the line of nucleophilic/electrophilic attack on C_1 and C_3 of the münchnones. To gauge the relative magnitude of the factors driving the regio-selectivities, the activation energies for all processes were decomposed using the distortion/interaction model (DIM)[83]. The interaction energies obtained within this scheme were further decomposed using Shubil Liu's (EDA-SBL) energy decomposition analysis[46–48]. All these analyses, as well as the NCI calculations, were performed using the Multiwfn software package[84].

Table 1: Experimental data reported by Lopchuk et. al.[32] for the studied cyclization reactions. For each of the corresponding dipole # - münchnone pair, the experimental syn:anti ratio of final products and the reaction yield is reported. For each syn:anti product case the corresponding TS is signaled.

	Münchnone A		**Münchnone B**	
dipolarophile #	syn:anti TSA:TSA'	yield (%)	syn:anti TSB':TSB	yield (%)
3	88:12	97	19:81	75
4	81:19	52	17:83	45
5	94:6	65	20:80	62
6	85:15	58	57:43	50
7	89:11	64	14:86	63
8	92:8	70	26:74	67
14	1:>99	83	>99:1	32

Results and discussion

As stated before, the studied reaction family has enormous potential in chemical synthesis. Previous attempts to rationalize the regio-selectivity of the present 13DC have failed, and no cDFT scheme for reactivity predictions has been successful in predicting the preferred regio-isomers from the reactants. The studied systems can be employed as a model to explore the causes behind these failures and help develop new predictive strategies/schemes for overcoming them. The developed strategies are expected to be useful for the reactivity rationalization of other problematic reactions (for example 13DC of nitrones). With that objective in mind, we seek to answer the following questions:

- Which are the preferred interactions present in the studied 13DC transition states?
- Are these interactions driving the 13DC regio-selectivity?
- Can global cDFT descriptors explain the 13DC regio-selectivity?
- Do steric effects affect the accuracy of cDFT predictions?
- What is the relative relevance of the key factors driving the regio-selectivity?

Which are the preferred interactions present in the studied 13DC transition states?

For all reactions, the TS geometries (corresponding to the major product) show a strong asynchronous character in the 13DC bond formation. As an illustrative example, Figure 3 depicts the TS geometries corresponding to the 13DC reactions for both münchnones and dipolarophiles 3 and 14.

For the reaction involving 3, the most prominent münchnone-dipole interaction involves the C_1 atom of the münchnone. We arrive at this conclusion for both münchnone A and B, as the TSs (TSA-3,TSB-3) show substantially shorter bond distances ($\sim 0.5\,\text{Å}$, $\sim 0.6\,\text{Å}$,

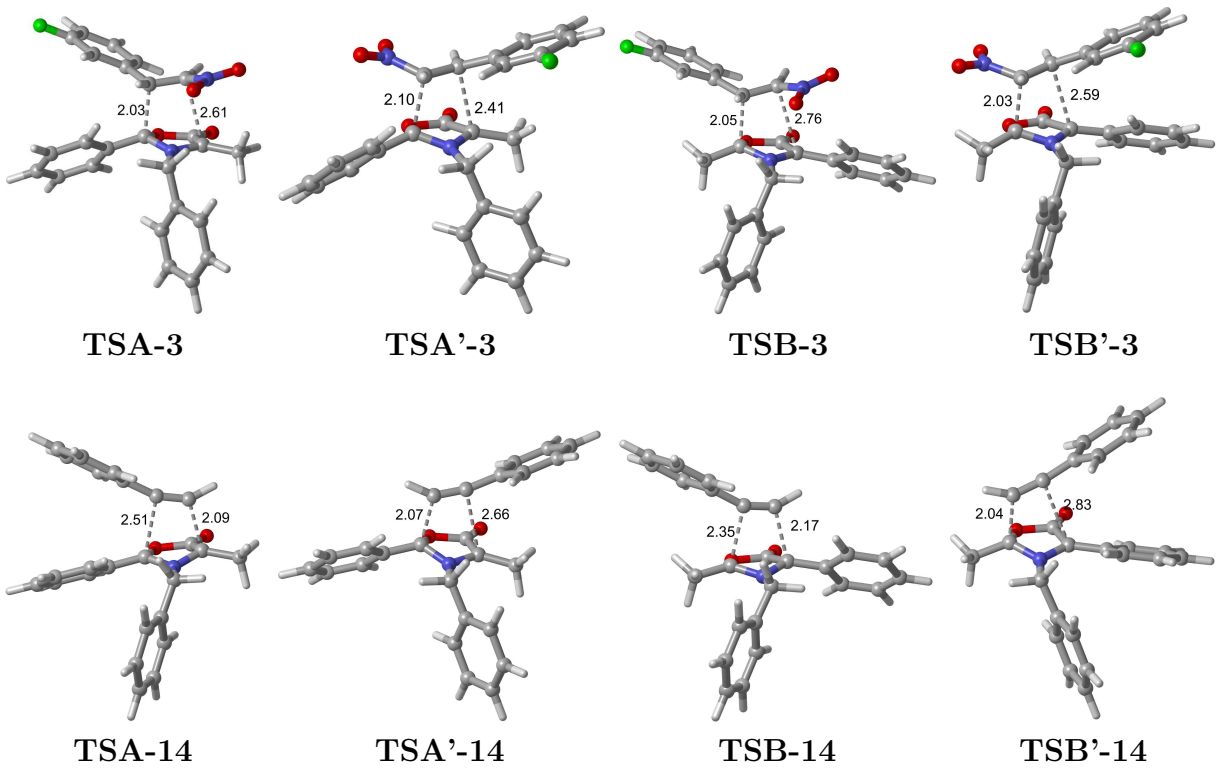

Figure 3: Geometries obtained for the TSs corresponding to the C_1-C_2 C_3-C_4 pairings of münchnone A (TSA) and münchnone B (TSB) with the different dipoles (numbers).

respectively) for the C_1 interaction than for the one involving C_3. For the TSs corresponding to the minor products (TSA'-3, TSB'-3), the bond distances differ on a lower scale ($\sim$ 0.3 Å, $\sim$ 0.5 Å, respectively), indicating a more synchronous evolution towards the products. Similar results were found for all the studied reactions (3-8) except for the one featuring dipole 14 (phenyl-acetylene). For this dipolarophile, the strongest interaction appears to be driven by the alkyne instead of the münchnone. The shorter münchnone-dipolarophile bond distance always features C_4 for all TSs (TSA-14, TSA'-14, TSB-14, and TSB'-14). Simultaneously, in all TS geometries, except for the reactions featuring dipolarophile 14, C_1 presents a deviation from its planar topology in the isolated münchnone. A possible origin of the modified geometry is a partial change from an sp^2 to an sp^3 hybridization. For the TSs featuring dipole 14, the planarity of the münchnone ring is more well preserved.

Are these interactions driving the 13DC regio-selectivity?

The Natural Bond Orbital (NBO) method represents the wave function using natural bond orbitals describing the electronic density of the system in terms of the most accurate Lewis-like structure possible. The orbitals resulting from the NBO method are more in consonance with a "chemical" description of the obtained molecular structure in terms of bonds and lone pairs. Moreover, the method provides second-order perturbation energies associated with charge transfer between orbitals (in line with the chemist's idea of donor-acceptor interactions)[85].

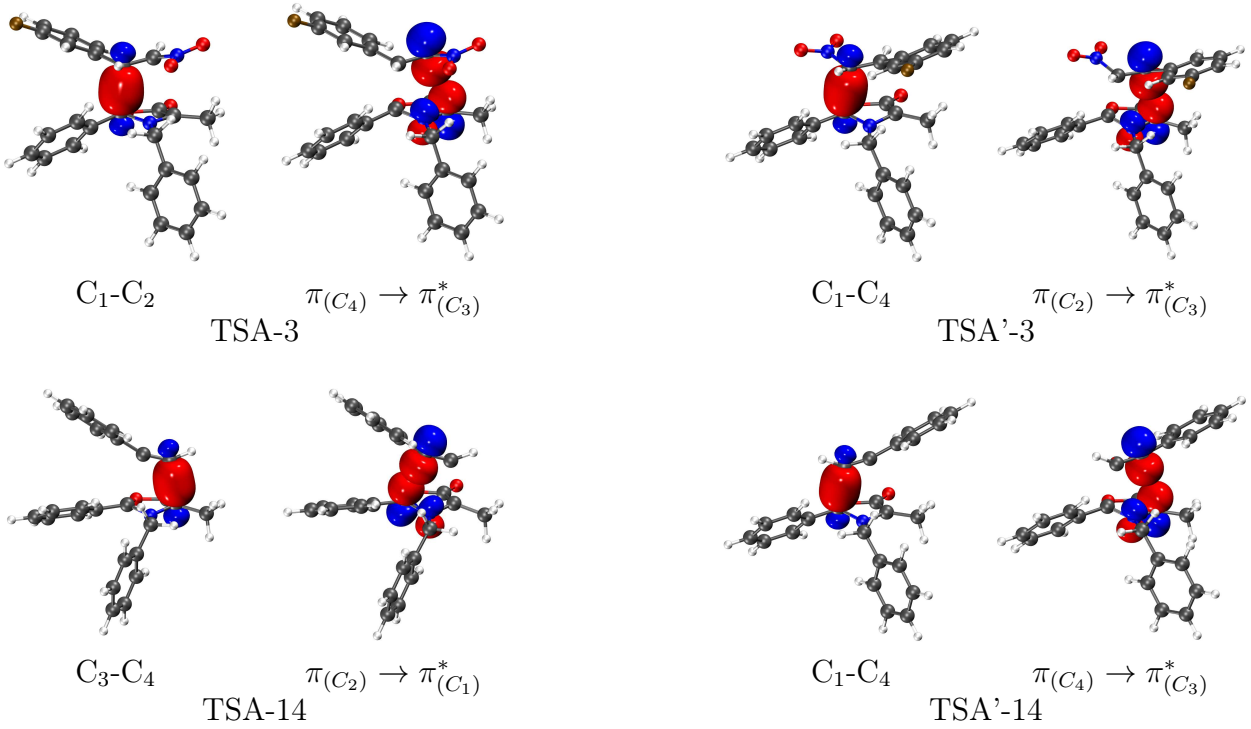

Figure 4: Geometries obtained for the TSs corresponding to the C_1-C_2 C_3-C_4 pairings of münchnone A (TSA) and münchnone B (TSB) with the different dipoles (numbers).

Figure 4 illustrates the NBO description of the most relevant dipole-dipolarophile interactions present in the TSs corresponding to the reactions featuring münchnone A and dipolarophiles 3 and 14. For both reactions, the TS corresponding to the major and minor products was analyzed.

For TSA-3 and TSA'-3, featuring dipole 3, the Lewis structure best describing the electronic

density represents the münchnone-dipolarophile interaction featuring C_1 as a σ bond. No bonding NBO was found for the corresponding interaction featuring münchnone C_3. Here instead, there is a donor-acceptor $\pi_{(C_4)} \rightarrow \pi^*_{(C_3)}$ interaction transferring electronic density from the dipolarophile to the münchnone (retro-donation-like characteristics). Similar results are observed for all reactions featuring any of the two münchnones and an alkene type dipolarophile (3-8).

Table 2: Orbital donor-acceptor interactions between the reactive atoms and their energy contributions in TSs corresponding to the C_1-C_2 C_3-C_4 pairings

	Interaction	$E^{(2)}$, kcal/mol		Interaction	$E^{(2)}$, kcal/mol
TSA-3	$\pi_{(C_4)} \rightarrow \pi^*_{(C_3)}$	23.4	TSB-3	$\pi_{(C_4)} \rightarrow \pi^*_{(C_3)}$	14.3
TSA-4	$\pi_{(C_4)} \rightarrow \pi^*_{(C_3)}$	6.6	TSB-4	$\pi_{(C_4)} \rightarrow \pi^*_{(C_3)}$	3.8
TSA-5	$\pi_{(C_4)} \rightarrow \pi^*_{(C_3)}$	21.9	TSB-5	$\pi_{(C_4)} \rightarrow \pi^*_{(C_3)}$	3.8
TSA-6	$\pi_{(C_4)} \rightarrow \pi^*_{(C_3)}$	26.7	TSB-6	$\pi_{(C_4)} \rightarrow \pi^*_{(C_3)}$	15.5
TSA-7	$\pi_{(C_4)} \rightarrow \pi^*_{(C_3)}$	22.4	TSB-7	$\pi_{(C_4)} \rightarrow \pi^*_{(C_3)}$	14.1
TSA-8	$\pi_{(C_4)} \rightarrow \pi^*_{(C_3)}$	24.6	TSB-8	$\pi_{(C_4)} \rightarrow \pi^*_{(C_3)}$	14.7
TSA-14	$\pi_{(C_2)} \rightarrow \pi^*_{(C_1)}$	284.6	TSB-14	$\pi_{(C_2)} \rightarrow \pi^*_{(C_1)}$	309.0

The NBO method yields similar results for complexes with dipolarophile 14 (TSA-14 and TSA'-14). In these cases, the münchnone-dipolarophile σ bond position was determined by the dipolarophile's orientation. More specifically, the NBO bond between the fragments always involves C_4, a persistent trend for münchnone B.

Table 3: Orbital donor-acceptor interactions between the reactive atoms and their energy contributions in TSs corresponding to the C_1-C_4 C_3-C_2 pairings

	Interaction	$E^{(2)}$, kcal/mol		Interaction	$E^{(2)}$, kcal/mol
TSA'-3	$\pi_{(C_2)} \rightarrow \pi^*_{(C_3)}$	96.0	TSB'-3	$\pi_{(C_2)} \rightarrow \pi^*_{(C_3)}$	51.1
TSA'-4	$\pi_{(C_2)} \rightarrow \pi^*_{(C_3)}$	96.0	TSB'-4	$\pi_{(C_2)} \rightarrow \pi^*_{(C_3)}$	53.1
TSA'-5	$\pi_{(C_2)} \rightarrow \pi^*_{(C_3)}$	122.1	TSB'-5	$\pi_{(C_2)} \rightarrow \pi^*_{(C_3)}$	57.6
TSA'-6	$\pi_{(C_2)} \rightarrow \pi^*_{(C_3)}$	58.0	TSB'-6	$\pi_{(C_2)} \rightarrow \pi^*_{(C_3)}$	33.9
TSA'-7	$\pi_{(C_2)} \rightarrow \pi^*_{(C_3)}$	115.8	TSB'-7	$\pi_{(C_2)} \rightarrow \pi^*_{(C_3)}$	57.7
TSA'-8	$\pi_{(C_2)} \rightarrow \pi^*_{(C_3)}$	83.8	TSB'-8	$\pi_{(C_2)} \rightarrow \pi^*_{(C_3)}$	41.5
TSA'-14	$\pi_{(C_4)} \rightarrow \pi^*_{(C_3)}$	78.4	TSB'-14	$\pi_{(C_4)} \rightarrow \pi^*_{(C_3)}$	181.2

The energy associated to the most important non-covalent inter-orbital interaction (between fragments), for each complex, are shown in Tables 2 and 3. Interestingly enough, when comparing donor-acceptor interaction energies (stabilizing) for the TSA-X with their corre-

sponding TSA'-X, the greatest interaction is always found for the less stable complex. This is a clear indication that donor-acceptor interactions are not the main factor contributing to the stabilization of the TSs and thus do not determine these reactions' regio-selectivity.

Non-covalent interactions can also be analyzed by means of the Reduced Density Gradient (RDG)[38,39]:

$$s(r) = \frac{1}{2(3\pi^2)^{1/3}} \frac{\nabla\rho(r)}{\rho(r)^{4/3}} \tag{21}$$

The RDG analysis focuses on plotting the regions with medium values for $s(r)$ that characterize the spatial distribution of the non-covalent interactions. For a more in-depth analysis of the strength and type of each interaction, an RDG vs. $\text{sign}(\lambda_2)\rho$ graph is employed. $s(r)$ is used to describe $\rho(r)$'s deviations from a homogeneous distribution, it exhibits very large positive values for regions far from the molecule and very small ones for regions of covalent interactions. In an s vs ρ graph, the non-covalent interactions will appear as steep troughs at low ρ values, corresponding to the density critical points that appear between the interacting atoms. At the same time, there is a positive correlation between the electron density of the critical points (ρ values where the trough appear) and the interaction strength. Furthermore, the sign of the second largest eigenvalue the electron density's Hessian matrix (λ_2) provides information about the type of interaction present ($\lambda_2 < 0$ attractive, $\lambda_2 > 0$ repulsive, $\lambda_2 \approx 0$ weak).

Figure 5 shows the NCI surfaces and RDG plots for the TSs corresponding to the major (TSA-3, TSB-3) and minor (TSA'-3, TSB'-3) products for the reactions of münchnones A and B with dipolarophile 3. By contrasting the NCI surfaces of TSA-3 with TSA'-3, or TSB-3 with TSB'-3, it can be seen that the variation of the interactions spatial distribution comprises mainly the weak (green) interactions. The strong repulsive (red) or attractive (blue) interaction distribution remains almost invariable. The repulsive interaction is localized between the münchnone ring and the dipolarophile double bond, while the attractive non-covalent interaction features münchnone C_3 (a result in line with the NBO interaction analysis).

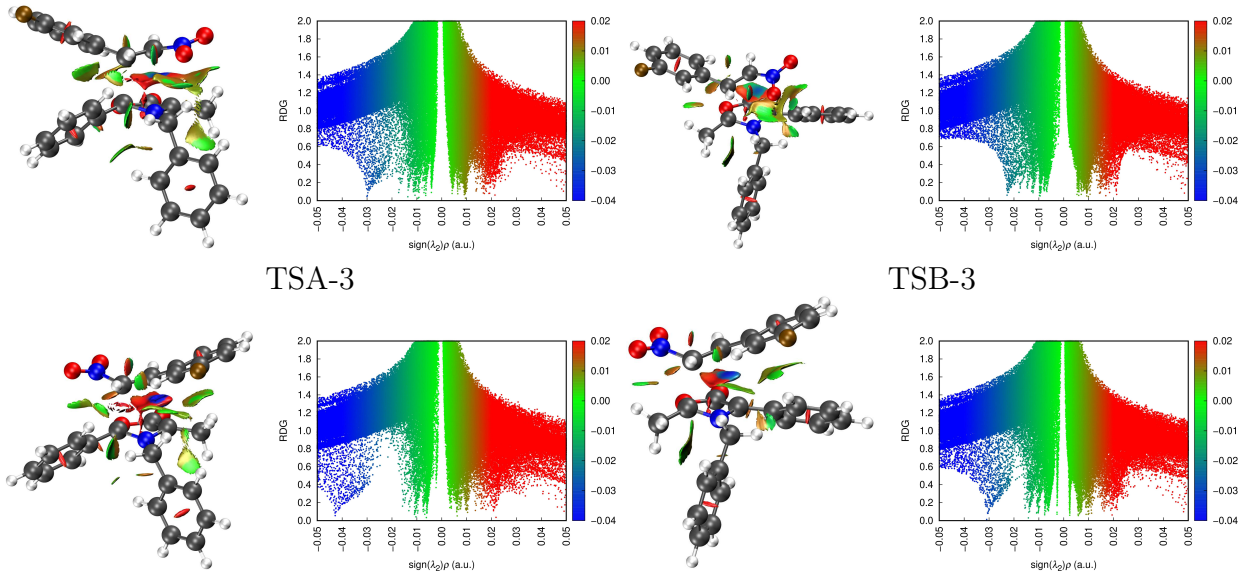

Figure 5: NCI interactions and RGD plots for all TSs involving dipolarophile 3.

On the other side, in the RDGscatter graphs, the strong attractive interaction (blue trough) is shifted towards higher $|\rho|$ values in TSA'-3 and TSB'-3 with respect to TSA-3 and TSB-3, respectively. This shift implies a stronger interaction (attractive) between monomers, and consequent greater stability for TSA'-3 and TSB'-3, which goes against the experimental products ratio (TSA-3 and TSB-3 are highly favored). The same results can be found for the rest of the studied TSs.

In hindsight, the trends found for the NBO interactions and NCI analysis indicate that the studied 13DC regio-selectivities are being governed by causes other than the electrostatic factors and non covalent interactions.

Can global cDFT descriptors explain the 13DC regio-selectivity?

First, we calculated the energies for the optimized geometries of the reactants and TSs, and the energies for the corresponding singly charged cations and anions (at the same geometry). These calculations allows us to obtain the (vertical) ionization and electron affinity energies employed to obtain the values for the global cDFT descriptors of interest. The

electronegativities (and other global descriptors) for the isolated dipoles and dipolarophiles are shown in Table 4. In all cases, the dipoles exhibit a lower electronegativity value; thus, the dipolarophile (alkene/alkyne) is predicted to behave as an acceptor of electronic density.

Table 4: Values for the global energy descriptors of interest for the isolated species. The values were obtained using the UB3LYP/6-311G(d,p) theory level.

	$\mu = -\frac{I+A}{2}$	$\chi = \frac{I+A}{2}$	$\eta = \frac{I-A}{2}$	$S = \frac{1}{2\eta}$	$\omega = \frac{\mu^2}{2\eta}$	$\varepsilon = \frac{1}{\omega}$
münchnone A	-0.122	0.122	0.117	4.268	0.064	15.632
münchnone B	-0.113	0.113	0.127	3.942	0.050	20.022
dipolarofile 3	-0.190	0.190	0.148	3.384	0.122	8.203
dipolarofile 4	-0.146	0.146	0.125	4.000	0.085	11.714
dipolarofile 5	-0.166	0.166	0.138	3.633	0.100	10.004
dipolarofile 6	-0.214	0.214	0.141	3.537	0.162	6.192
dipolarofile 7	-0.176	0.176	0.143	3.494	0.109	9.188
dipolarofile 8	-0.199	0.199	0.147	3.393	0.134	7.436
dipolarofile 14	-0.143	0.143	0.173	2.895	0.059	16.900

.

Natural charges were estimated for both species within the TS complexes to assess the magnitude and direction of charge transfer between the münchnones and dipolarophiles in the corresponding TSs. The results shown in Table 5, were consistent with the predictions based on χ. Without exception, the dipole acted as the donor of electronic density and the dipolarophile as the acceptor. It is noteworthy the lower magnitude of the charge transfer for the TSs involving dipolarophile 14. In these cases, the charge transfer represents at most half the transfer occurring for other dipolarophiles.

Table 5: Natural charges for the dipole and dipolarophile in all calculated TSs. The values were obtained using the UB3LYP/6-311G(d,p) theory level.

	TSA		TSA'		TSB		TSB'	
	Dipole	Dipolarophile	Dipole	Dipolarophile	Dipole	Dipolarophile	Dipole	Dipolarophile
3	0.327	-0.327	0.257	-0.257	0.331	-0.331	0.227	-0.227
4	0.306	-0.306	0.197	-0.197	0.309	-0.309	0.134	-0.134
5	0.313	-0.313	0.221	-0.221	0.316	-0.316	0.173	-0.173
6	0.342	-0.342	0.342	-0.342	0.349	-0.349	0.281	-0.281
7	0.316	-0.316	0.234	-0.234	0.319	-0.319	0.194	-0.194
8	0.332	-0.332	0.270	-0.270	0.337	-0.337	0.249	-0.249
14	0.163	-0.163	0.102	-0.102	0.164	-0.164	0.065	-0.065

The accuracy relation for the reactivity principles, based on global cDFT descriptors, pre-

dicting the major product for all studied reactions is shown in Table 6. The best performance was achieved for the "Maximum hardness" principle, giving an accurate prediction in 8 of 14 cases, followed by the "$\Delta|\mu|$ big is good" with 7 accurate predictions. The "minimum electrophilicity"-based predictions were wrong for all the reactions.

Table 6: Capability of the global cDFT reactivity criteria to predict the correct major product for the reactions of the different dipolarophiles with the münchnones A and B.

	TSA/TSA'			TSB/TSB'		
	$\Delta\|\mu\|$ big is good	Max. η	Min. ω	$\Delta\|\mu\|$ big is good	Max. η	Min. ω
3	bad	bad	bad	good	good	bad
4	bad	bad	bad	good	good	bad
5	good	bad	bad	good	good	bad
6	good	good	bad	bad	bad	bad
7	bad	bad	bad	good	good	bad
8	bad	good	bad	good	good	bad
14	bad	good	bad	bad	bad	bad

Global descriptors can predict the preferred regio-isomer, but the TS geometry must be calculated first. Local descriptors (with a matching criteria) are commonly employed as an alternative to regio-selectivity predictions from the reactants properties.

As in all reactions, münchnones act as electron donor, their reactivity should be determined by the location of $f^-(r)$. Meanwhile, the reactive sites for the dipolarophiles should be determined by $f^+(r)$. Factoring these elements, the major predicted regio-isomer is the one obtained by matching münchnone biggest $f^-(r)$ lobe with the dipolarophile's biggest $f^+(r)$ lobe.

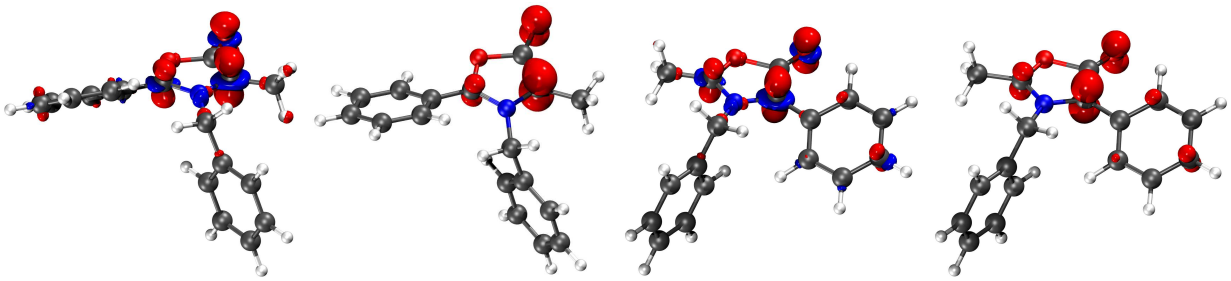

A-FD A-GGV B-FD B-GGV

Figure 6: $f^-(r)$ isosurfaces calculated for the münchnones A and B using the FD (0.007 a.u.) and GGV (0.012 a.u.) approximations.

Figure 6 displays the $f^{-}(r)$ isosurfaces for münchnones A and B, obtained by the FD (0.007 a.u.) and GGV (0.012 a.u.) approximations. The GGV approach conduces to smoother and less complicated isosurfaces, but the core results from both approaches show no significant differences. For the two münchnones, $f^{-}(r)$ appears mostly located over C_3 being predicted as the most important reactive (electron donor) site. This result is inconsistent with the geometries obtained for the TSs corresponding to the major products, where except for the reaction 14 (for which the most important interaction appears to be defined by the alkyne C_4), the dominant interaction always involves münchnone C_1 atom (Figure 3).

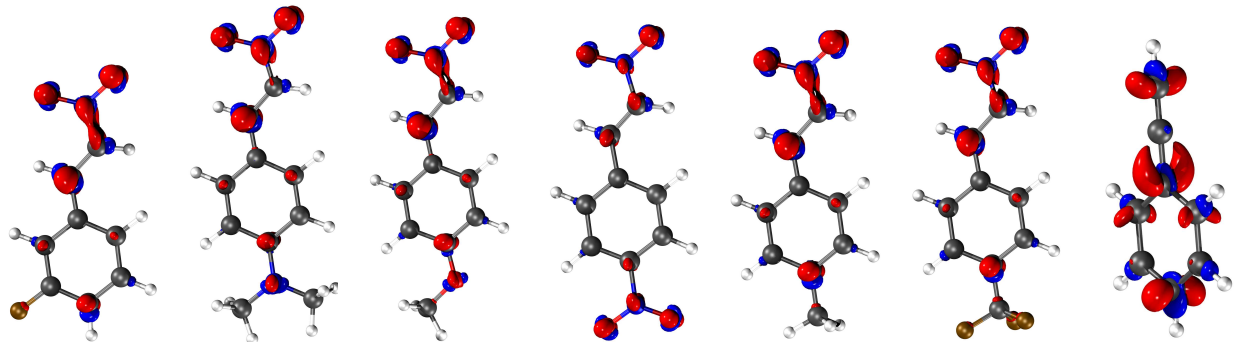

Figure 7: $f^{+}(r)$ isosurfaces calculated for the dipolarophiles using the FD (0.007 a.u.) approximation.

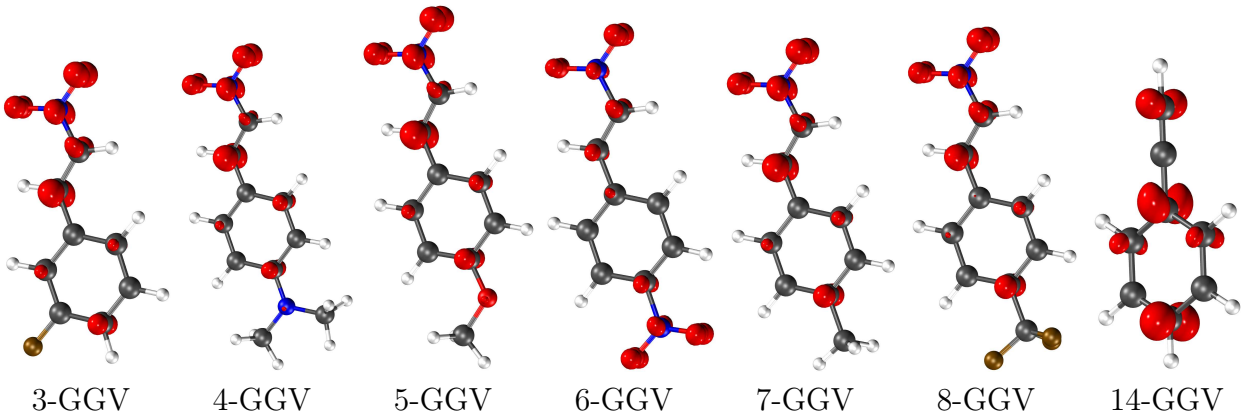

Figure 8: $f^{+}(r)$ isosurfaces calculated for the dipolarophiles using the GGV (0.012 a.u.) approximations.

The $f^{+}(r)$ isosurfaces calculated for the dipolarophiles using the FD (0.007 a.u.) and GGV (0.012 a.u.) schemes are shown in Figure 7 and Figure 8, respectively. Both approaches yield

the same qualitative results, being the GGV isosurfaces simpler and easier to interpret. C_2 is predicted as the more electrophilic carbon in the reacting insaturation for all cases except the dipolarophile 6 and dipolarophile 14. For dipolarophile 6, both C atoms on the insaturation are predicted to be equally reactive with a slightly bigger lobe on the C_4. Meanwhile, for dipolarophile 14, the trend reverts. These results perfectly agree with the more reactive dipolarophile C atoms in the predicted TSs geometries for the major products. Nonetheless, when paired with the inconsistent prediction of the donor C_3 atom in the münchnones, the pairing of the $f(r)$ lobes fails to reproduce the experimental results in all cases but for the reaction of münchnone A with dipolarophile 6. The results are summarized in Table 7, together with the predicted products' accuracy compared with the experimental results.

Figure 9 depicts the münchnones' $\Delta f(r)$ isosurfaces calculated using FD and GGV approximations. $\Delta f(r)$'s isosurfaces are more complicated than those of $f(r)$ as they comprise more information. GGV isosurfaces are simpler than FD's. In general, the first ones tend to have fewer lobes; usually, all lobes centered on the same atom have equal signs.

For both münchnones $\Delta f(r)$ tends to concentrate on C_3, with the lobes featuring a negative sign. This behavior corresponds to electron donor character. The case of C_1 shows no strongly defined donor/acceptor character (using his set of isovalues). A notable exception occurs for münchnone A with $\Delta f(r)$ obtained using the FD approximation. Here C_1 is also predicted to present electron donor character, although of lesser magnitude than C_3. These results coincide with those obtained using $f(r)$: the most relevant interaction involving C_3,

Table 7: Accuracy of predictions for the major product by pairing the münchnone $f^-(r)$ and dipolarophile $f^+(r)$ functions.

	Münchnone A		**Münchnone B**	
Dipolarophile	FD	GGV	FD	GGV
3	bad	bad	bad	bad
4	bad	bad	bad	bad
5	bad	bad	bad	bad
6	good	good	bad	bad
7	bad	bad	bad	bad
8	bad	bad	bad	bad
14	bad	bad	bad	bad

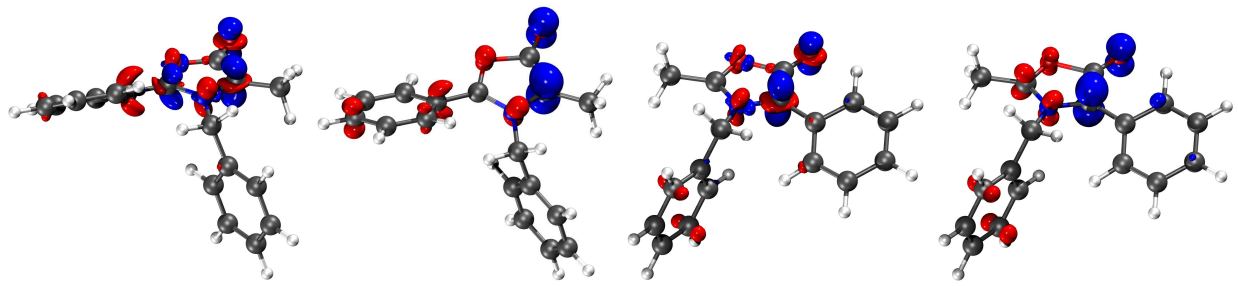

A-FD A-GGV B-FD B-GGV

Figure 9: $\Delta f(r)$ isosurfaces (positive sign in red and negative sign in blue) calculated for the münchnones A and B using the FD (0.007 a.u.) and GGV (0.012 a.u.) approximations.

which is inconsistent with the predicted TS geometries for the major products.

Figures 10 and 11 show $\Delta f(r)$ for all dipolarophiles calculated with the FD and GGV approaches, respectively. The FD and GGV isosurfaces show similar qualitative results, with the latter being simpler and the donor/acceptor character for each atom easily defined.

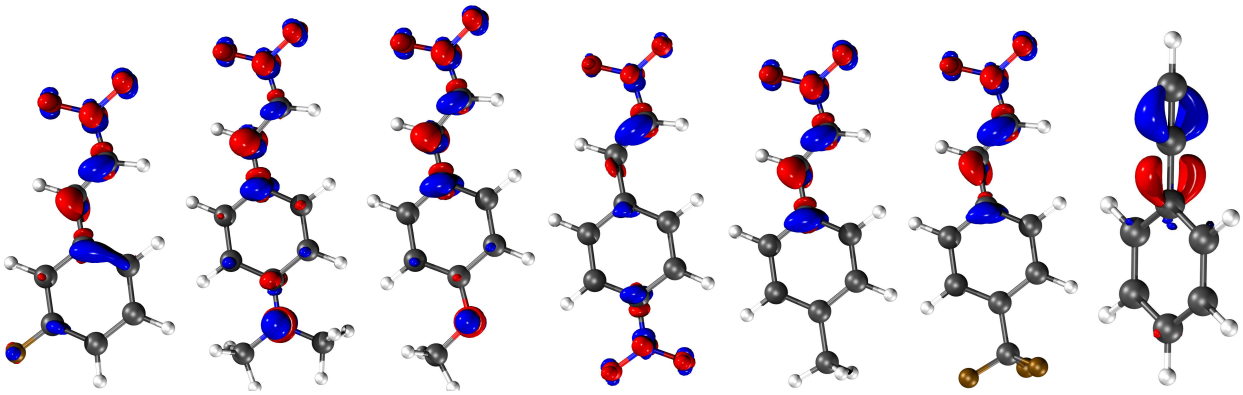

3-FD 4-FD 5-FD 6-FD 7-FD 8-FD 14-FD

Figure 10: $\Delta f(r)$ isosurfaces (positive sign in red and negative sign in blue) calculated for the dipolarophiles using the FD (0.007 a.u.) method.

For the dipolarophiles, in all cases, the C_2 exhibits lobes with positive $\Delta f(r)$ values corresponding to an electron acceptor character. These results predict the most critical dipole-dipolarophile interaction features C_2, with the dipolarophile expected to perform as an electron acceptor. This conclusion agrees with the geometrical and electron density analysis performed for the TSs. In the case of C_4, the lobes are almost in all cases of negative sign. Meanwhile, dipolarophile 14 (phenylacetylene) presents lobes of both characters; nonetheless, in all cases, C_2 is expected to act as a better electron donor than C_4.

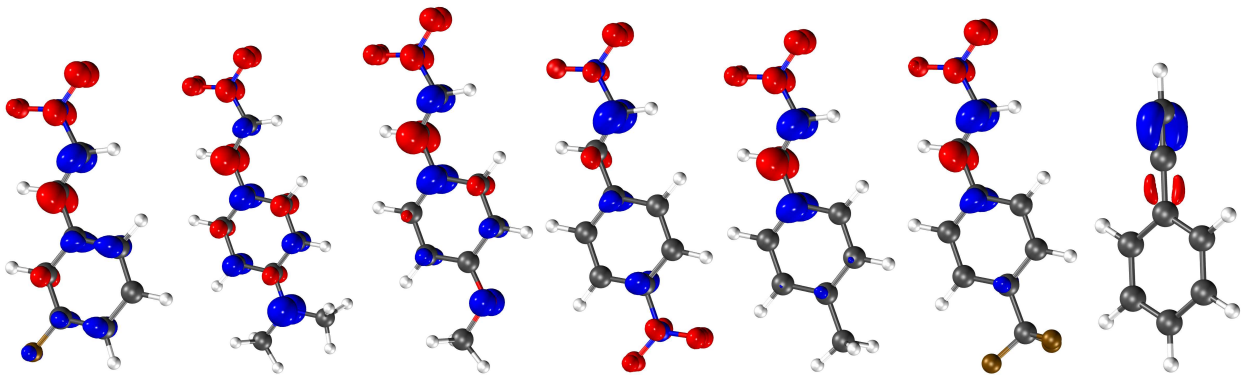

Figure 11: $\Delta f(r)$ isosurfaces (positive sign in red and negative sign in blue) calculated for the dipolarophiles using the GGV (0.012 a.u.) method.

The predicted product is obtained by matching the $\Delta f(r)$ lobes of a molecule with the lobes featuring a different sign from the other molecule. For these reactions, the predicted major product corresponds to the bonding of C_1 with C_4 and C_2 with C_3 (anti for münchnone A and syn for münchnone B). This reasoning fails to predict the experimental major product for all but three cases out of 14, as depicted in Table 8.

Table 8: Accuracy of predictions for the major product by pairing the $\Delta f(r)$ of münchnone and dipolarophile lobes.

	Münchnone A		**Münchnone B**	
Dipolarophile	FD	GGV	FD	GGV
3	bad	bad	bad	bad
4	bad	bad	bad	bad
5	bad	bad	bad	bad
6	bad	bad	good	good
7	bad	bad	bad	bad
8	bad	bad	bad	bad
14	good	good	good	good

Table 9 illustrates the accuracy of the predicted major regio-isomer compared to the experimental results.

The condensation of $f(r)$ and $\Delta f(r)$ in atomic quantities does not substantially improve the accuracy of the predictors. Even more, estimates based on the quantities f_k and Δf_k fail to predict the major isomer for all but one reaction, a significant deterioration from the visual analysis results.

Table 9: Accuracy of predictions based on condensed $f(r)$ and $\Delta f(r)$ descriptors. For $\Delta f(r)$, the accuracy of its predictions is also shown when condensing only the domains relevant to the reactivity.

	Condensed f_k		Condensed Δf_k		Domain $\Delta f(r)$ (FD)		Domain $\Delta f(r)$ (GGV)	
	A	B	A	B	A	B	A	B
3	bad	bad	bad	bad	bad	bad	bad	bad
4	bad	bad	bad	bad	bad	bad	bad	bad
5	bad	bad	bad	bad	bad	bad	bad	bad
6	bad	good	bad	good	bad	bad	good	good
7	bad	bad	bad	bad	bad	bad	bad	bad
8	bad	bad	bad	bad	bad	bad	bad	bad
14	bad	bad	bad	bad	good	good	good	good

The integration, for $\Delta f(r)$, of only the domains (lobes) relevant to the reactivity only provides a marginal improvement of the predictive capabilities of this descriptor. The best case scenario is achieved by mixing this approach with the GGV based $\Delta f(r)$. This procedure only predicts the correct regio-isomer in 4 out of 14 cases.

The pairing of the local/atomic softness values was the local descriptor that best describes the regio-selectivity of the studied reactions. In all TSs, münchnones act as donor, then the reactivity of its atoms (C_1, C_3) should be determined by s_i^-. Consequently, s_i^+ determines the reactivity for the dipolarophile reactive atoms (C_2, C_4) acting as electron acceptor.

Table 10 displays the more favored interaction münchnone-dipolarophile for each reaction together with the accuracy of the predicted product. The local softness accurately predicts the major regioisomer and the most relevant dipole-dipolarophile interaction for 12 out of 14 cases, being accurate for the 85% of cases.

Another alternative is to assume the regio-selectivity is not led by the interaction of two atoms but to consider the HSAB principle for all reactive atoms in a democratic way. Hence, we can define the following descriptors:

$$HSAB_{C_1-C_2,C_3-C_4} = (s_{C_1}^- - s_{C_2}^+)^2 + (s_{C_3}^- - s_{C_4}^+)^2 \cdot S \tag{22}$$

$$HSAB_{C_1-C_4,C_3-C_2} = (s_{C_1}^- - s_{C_4}^+)^2 + (s_{C_3}^- - s_{C_2}^+)^2 \cdot S \tag{23}$$

Table 10: More favored pair interaction according to local softness following HSAB and the accuracy for the corresponding predicted product. The values were obtained using the UB3LYP/6-311G(d,p) theory level.

	Predicted Pair		Predicted Product	
	münchnone A	münchnone B	münchnone A	münchnone B
dipolarophile 3	$1\cdots2$	$1\cdots2$	good	good
dipolarophile 4	$1\cdots2$	$1\cdots2$	good	good
dipolarophile 5	$1\cdots2$	$1\cdots2$	good	good
dipolarophile 6	$1\cdots2$	$1\cdots2$	good	bad
dipolarophile 7	$1\cdots2$	$1\cdots2$	good	good
dipolarophile 8	$1\cdots2$	$1\cdots2$	good	good
dipolarophile 14	$1\cdots4$	$3\cdots4$	good	bad

Table 11: Accuracy of predictions for the major product with the HSAB descriptor.

	münchnone A	münchnone B
dipolarophile 3	bad	bad
dipolarophile 4	bad	bad
dipolarophile 5	bad	bad
dipolarophile 6	bad	good
dipolarophile 7	bad	bad
dipolarophile 8	bad	bad
dipolarophile 14	bad	bad

Here $HSAB_{C_1-C_2,C_3-C_4}$ corresponds to the interaction C_1-C_2 and C_3-C_4, while $HSAB_{C_1-C_4,C_3-C_2}$ corresponds to the match C_1-C_4 and C_3-C_2. For each münchnone-dipolarophile pair, the HSAB descriptor with the lowest value indicates the preferred regioisomer. Table 11 shows the accuracy of the predictions obtained using the HSAB descriptor. The descriptor fails to predict the correct major product for all but one case.

Since the $f(r)$ and $\Delta f(r)$ local descriptors fail to reproduce the correct reactivity preference of the münchnone C_1 and C_3, an alternative local descriptor was also considered. The average local ionization energy[86] $\overline{I}(R)$, which provides a local measure to the ionization potential. It can be calculated as:

$$\overline{I}(r) = \frac{\sum_i \rho_i(r)|\varepsilon_i|}{\rho(r)} \tag{24}$$

Higher $\overline{I}(R)$ values correspond to points where the electron density is more tightly bonded, and lower values indicate points with a more weakly bonded electronic density. Taking this into account, it results natural that the minima of $\overline{I}(R)$ on a vdW surface correspond to

the atoms more prone to suffer from an electrophilic attack. Then, $\overline{I}(R)$ can be seen as an alternative to $f^{-}(r)$ in predicting the regio-selectivity of the reactions[87].

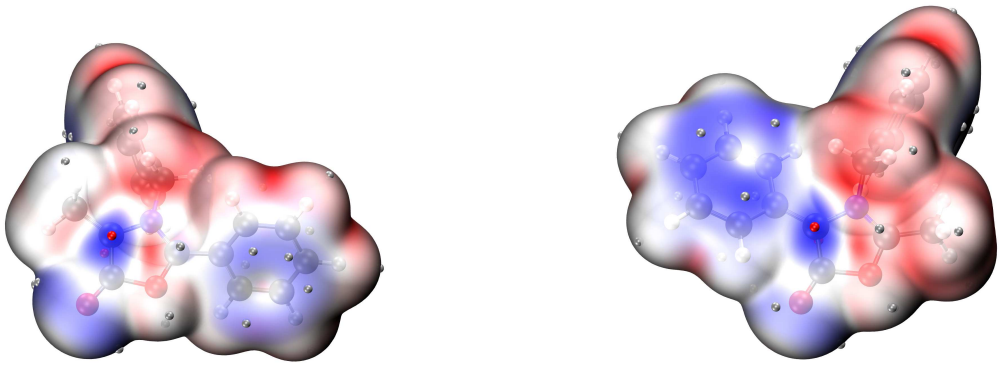

Münchnone A Münchnone B

Figure 12: $\overline{I}(R)$ values mapped on the vdW isosurface corresponding to $\rho = 0.001$. The red areas correspond to higher values and the blue areas correspond to lower values. The small silver color spheres on the surface correspond to local minima and the small red sphere to the global minimum.

Figure 12 displays the $\overline{I}(R)$ calculated values mapped on the isosurface corresponding to $\rho = 0.001$ a.u., a value commonly used to define the molecular van der Waals (vdW) surface. Red areas correspond to higher values of $\overline{I}(R)$ while lower values areas appear in blue. The small silver-colored spheres embedded into the surface represent the local minima of $\overline{I}(R)$ on the vdW surface. Meanwhile, the global minimum is marked with a red-colored sphere. For both münchnones, the global $\overline{I}(R)$ minima is directly situated above the C_3 atom. This result coincides with the previous descriptors ($f(r)$, $\Delta f(r)$), and, as with the other cases, it fails to predict the preferred reactive site depicted by the TS geometries corresponding to the major products.

Do steric interactions affect the accuracy of cDFT predictions?

From all local reactivity descriptors previously analyzed, only the matching of condensed softness in line with the HSAB principle (predicting the most favored C-C münchnone-

dipolarophile interaction) yields accurate predictions for each reaction's major product. This descriptor not only accurately predicts the major regio-isomer, but, at the same time, the predicted more favored C-C interactions are in line with the results shown by the geometrical and electronic density analysis of the TSs.

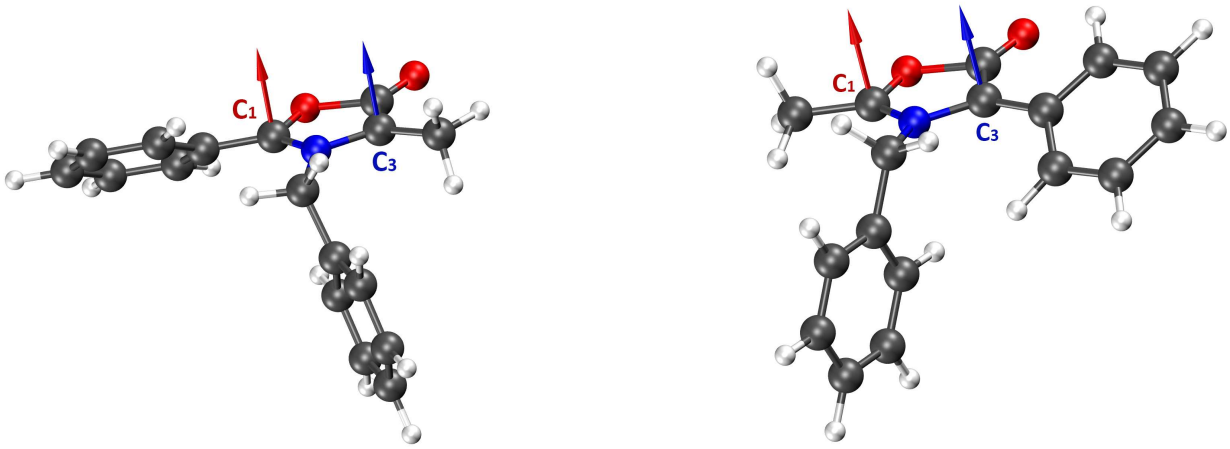

Figure 13: Steric force evolution along lines perpendicular to the münchnone ring centered in the reacting atoms.

An opposite result is found for the local descriptors based on the electronic density susceptibility to suffering electrophilic/nucleophilic attacks ($f(r)$, $\delta f(r)$, and ALIE). For these, the dipolarophile predicted C atom participating in the most important (dipole-dipolarophile) interaction (most significant electron acceptor character) is in line with the results found for the TSs geometry and $\rho(r)$ analysis. For both münchnones, the predicted more reactive atom (most significant electron donor character) is inconsistent with the TSs geometry and $\rho(r)$ analysis. As a result, the combination leads to wrong product prediction for almost all cases.

It is necessary to note that for both münchnones, the less reactive C atom is predicted to exhibit the same (donor) character but on a lesser magnitude. This atom could, in principle, also favorably interact with the electron acceptor atom (the magnitude of the interaction should be lesser nonetheless) of the dipolarophile (predicting the correct regio-isomer). These observations suggest the presence of other factors (probably steric repulsion) offsetting the

preferred interactions predicted by cDFT descriptors.

As a measure of how much, the electrophilic attacks on the münchnones reactive atoms, are sterically impeded, the magnitude of the steric force was calculated along the direction of the attacks (shown in Figure 13). The results for C_1 and C_3 are shown in Figure 14.

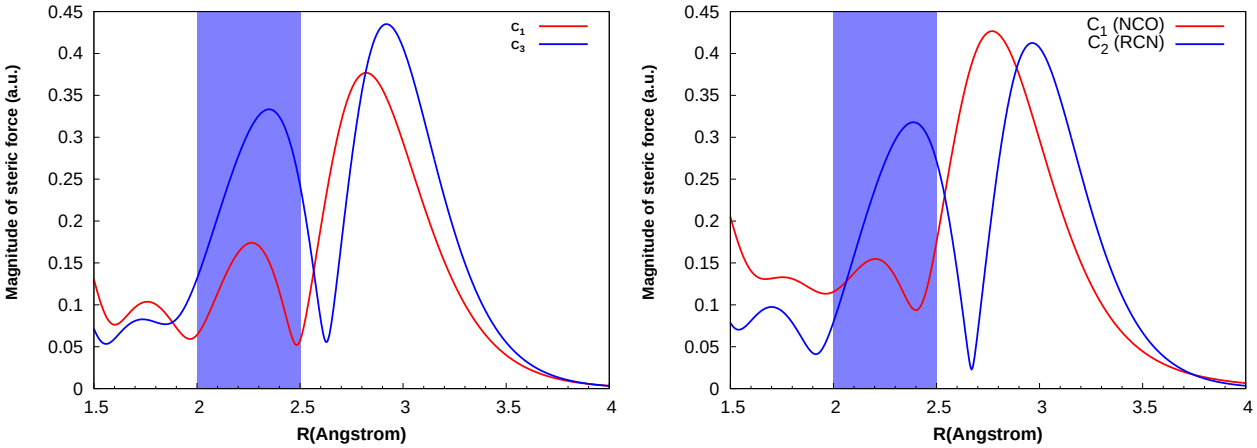

Figure 14: Steric force evolution along lines perpendicular to the münchnone ring centered in the reacting atoms.

The complex dependence of the steric force on the distance to the centers can be easily noted. Our analysis is centered in the region from 2.0 to 2.5 Åcovering C-C distances between the reactive atoms present in the TSs, and thus where the interactions determine the activation energy and regio-selectivity. For this distance interval, C_1 has the lower steric force and thus is less sterically hindered and, consequently, more available to an electrophilic attack. If these criteria (C_1 will be the münchnone best nucleophilic atom as it is less sterically impeded) are factored, the correct regio-isomer is accurately predicted (by $f(r)$ and $\Delta f(r)$) for all cases except dipole B with dipolarophile 6. This last case has practically no regio-selectivity; thus, an accurate prediction is of no significance.

What are the relative relevance of the key factors driving the regio-selectivity?

For a quantitative estimation of regioisomer yield ratios, highly accurate barrier values are needed and thus is necessary to estimate the solvent effects on the involved species. Nonetheless, even without considering solvent effects, barrier estimations can provide qualitative predictions on the major product and the factors driving the regio-selectivity of the cycloaddition.

The total activation energies are decomposed using the distortion/interaction model[83] (DIM) to assess the main factors determining the barrier heights and, thus, the regio-selectivities. Here the total activation energy is separated into distortion and interaction energy terms.

$$\Delta E_a = \Delta E^{(\text{dist})} + \Delta E^{(\text{int})} \tag{25}$$

The distortion term is the energy necessary to distort the isolated reactants to their geometrical arrangements in the pre-reactive (TS) complex and can be expressed as the sum of the distortion energy for each of the reactants:

$$\Delta E_X^{(\text{dist})} = E_x^{(\text{complex})} + E_x^{(\text{isolated})} \tag{26}$$

Here $E_x^{(\text{complex})}$ represents the energy of molecule x in the TS's distorted geometry and $E_x^{(\text{isolated})}$ represents the energy corresponding to x in its relaxed geometry.

The interaction energy can be calculated, using the supramolecular approximation (employing the distorted reactants) and subsequently partitioned into its components using an energy decomposition analysis scheme. We used the partition scheme proposed by Shubin Liu[46–48] (EDA-SBL) which separates the energy of a molecule in three components (steric,

electrostatic and quantum):

$$E = E_{\text{steric}} + E_{\text{electrostatic}} + E_{\text{quantum}} \tag{27}$$

The interactions for the TSs corresponding to the major and minority products were compared using the difference in "activation energy" ($\Delta\Delta E_a$) and its DIM-EDA decomposition providing insights into the forces driving the regio-selectivity of these 13DC.

$$\begin{aligned}\Delta\Delta E_a &= \Delta E_a(TSX') - \Delta E_a(TSX) \\ &= \Delta\Delta E_{\text{distortion}} + \Delta\Delta E_{\text{steric}} + \Delta\Delta E_{\text{electrostatic}} + \Delta\Delta E_{\text{quantum}}\end{aligned}$$

The results are shown in Table 12.

Table 12: Variations on the EDA-SBL interaction components ($\text{kcal} \cdot \text{mol}^{-1}$) for the TSs corresponding to the major and minor products respectively.

	$\Delta E(TSA'_X) - \Delta E(TSA)_X$						$\Delta E(TSB'_X) - \Delta E(TSB)$					
	$\Delta\Delta E_{\text{st}}$	$\Delta\Delta E_{\text{el}}$	$\Delta\Delta E_{\text{qt}}$	$\Delta\Delta E^{\text{dip.}}_{\text{dist}}$	$\Delta\Delta E^{\text{münch.}}_{\text{dist}}$	$\Delta\Delta E_{\text{tot}}$	$\Delta\Delta E_{\text{st}}$	$\Delta\Delta E_{\text{el}}$	$\Delta\Delta E_{\text{qt}}$	$\Delta\Delta E^{\text{dip.}}_{\text{dist}}$	$\Delta\Delta E^{\text{münch.}}_{\text{dist}}$	$\Delta\Delta E_{\text{tot}}$
3	65.3	16.1	-75.6	1.2	0.0	7.0	30.2	4.8	-31.2	0.9	0.9	6.9
4	72.7	18.5	-84.2	1.0	-0.8	7.1	35.9	4.5	-35.3	1.5	-0.2	6.9
5	71.3	18.4	-83.1	1.2	-0.1	7.5	31.2	4.4	-31.2	2.4	0.7	7.4
6	70.0	17.0	-79.9	0.1	-0.5	6.9	40.0	5.3	-40.6	2.7	0.4	6.1
7	67.6	16.8	-78.4	1.3	0.0	7.2	30.5	4.7	-31.2	0.9	0.9	7.3
8	67.7	16.2	-77.5	0.9	0.0	7.3	16.1	3.4	-15.8	2.7	0.8	6.4
14	-16.1	-2.0	17.6	-0.7	-2.9	-4.1	17.3	5.6	-18.5	-0.6	-4.0	-1.2

For all studied TSs, the contributions to the interaction that undergoes the greatest changes from TS to TS' are the $\Delta\Delta E_{\text{qt}}$ closely followed by $\Delta\Delta E_{\text{st}}$ and on a second plane $\Delta\Delta E_{\text{el}}$. Distortion effects are practically the same for both regioisomers, not significantly affecting the regio-selectivity of the ciclo-addition. On the other hand, the steric and electrostatic effects rationalize correctly the experimental regio-selectivity (the former of a much bigger magnitude). This conclusion is consistent with all previous analyses indicating that electrostatic effects are not the regio-selectivity biggest driving force and pointing to steric effects as the major responsible for the regio-selectivity.

For müchnone A both the steric and electrostatic effects rationalize the regio-selectivity correctly. That is, for the TS of the major product, the electrostatic attraction is favored, and there is less steric repulsion for all cases but for the interaction with the alkyne. In the case of munchnone B, the same trend is observed. A mixture of steric and electrostatic effects accurately accounts for the regio-selectivity in all cases but the ciclo-addition with dipolarophile 6 and 14.

Conclusions

The regio-selectivity for the 13DC of two münchnones with a test set of alkenes and one alkyne was accurately rationalized by employing B3LYP/6-311G** calculations, cDFT descriptors, and steric force analysis. The most relevant interaction was determined for all 13DCs by means of the TS geometry, and electronic density (within the NBO and NCI frameworks) analyses. For all münchnone-alkene reactions, this interaction features münchnone's C_1 regardless of the dipolarophile orientation (anti/syn). For the case of the alkyne 13DC, the interaction features alkyne's C_4 regardless of the münchnone orientation. For all cases, the non-covalent attractive interactions fail to reproduce the regio-selectivity and thus indicates other factors are in play.

Global descriptors have little success predicting the major products, the best performer being the maximum hardness principle with roughly 50% of accuracy. For local descriptors, the pairing of the atomic softness following the HSAB principle was found to accurately predict the regio-selectivity for almost all 13DCs failing only in two cases out of 14 (also for one of the cases the experimental results indicate a minimal regio-selectivity). The Fukui function and dual descriptor fail to reproduce the correct regio-selectivity for almost all cases. If the steric repulsion is taken into account (offsetting the reactivity priorities for münchnone C_1C and C_3) both methods perform with remarkable accuracy (the predictions are reversed and only one case of 14 fails). Steric effects are similar for münchnone A and B, indicating the

Ph poses no big steric impediment to the attacking dipolarophile. This can be understood as the ring adopting a co-planar orientation with the münchnone ring. The relative relevance of the present interactions in the TS was assessed using an energy decomposition analysis of the interactions, steric effect playing a major role.

In general, the cDFT local descriptors, when paired with the münchnone's rationalization of the steric effects successfully rationalize the experimental results. It is expected that the strategy of combining steric and cDFT aspects helps to understand and predict the regio-selectivity of other problematic systems of interest, such as 13DC of nitrones.

References

(1) Nathaniel, C. R.; Neetha, M.; Anilkumar, G. Silver-catalyzed pyrrole synthesis: An overview. *Applied Organometallic Chemistry* **2021**, *35*, e6141, e6141 aoc.202001412.R1.

(2) Ju, Y.; Varma, R. S. Aqueous N-heterocyclization of primary amines and hydrazines with dihalides: microwave-assisted syntheses of N-azacycloalkanes, isoindole, pyrazole, pyrazolidine, and phthalazine derivatives. *The Journal of organic chemistry* **2006**, *71*, 135–141.

(3) Liang, Q.; Hayashi, K.; Song, D. Reactivity of an Unprotected Mesoionic N-Heterocyclic Olefin. *Organometallics* **2020**, *39*, 4115–4122.

(4) Dumrath, A.; Wu, X.-F.; Neumann, H.; Spannenberg, A.; Jackstell, R.; Beller, M. Recyclable Catalysts for Palladium-Catalyzed C-O Coupling Reactions, Buchwald–Hartwig Aminations, and Sonogashira Reactions. *Angewandte Chemie International Edition* **2010**, *49*, 8988–8992.

(5) Vitaku, E.; Smith, D. T.; Njardarson, J. T. Analysis of the Structural Diversity, Substitution Patterns, and Frequency of Nitrogen Heterocycles among U.S. FDA Approved Pharmaceuticals. *J. Med. Chem.* **2014**, *57*, 10257–10274.

(6) Petri, G. L.; Spanò, V.; Spatola, R.; Holl, R.; Raimondi, M. V.; Barraja, P.; Montalbano, A. Bioactive pyrrole-based compounds with target selectivity. *European journal of medicinal chemistry* **2020**, *208*, 112783.

(7) Bhutani, P.; Joshi, G.; Raja, N.; Bachhav, N.; Rajanna, P. K.; Bhutani, H.; Paul, A. T.; Kumar, R. U.S. FDA Approved Drugs from 2015–June 2020: A Perspective. *Journal of Medicinal Chemistry* **2021**, *64*, 2339–2381, PMID: 33617716.

(8) Estévez, V.; Villacampa, M.; Menéndez, J. C. Recent advances in the synthesis of pyrroles by multicomponent reactions. *Chemical Society Reviews* **2014**, *43*, 4633–4657.

(9) Firsov, A. M.; Khailova, L. S.; Rokitskaya, T. I.; Kotova, E. A.; Antonenko, Y. N. Antibiotic Pyrrolomycin as an Efficient Mitochondrial Uncoupler. *Biochemistry (Moscow)* **2022**, *87*, 812–822.

(10) Raimondi, M. V.; Listro, R.; Cusimano, M. G.; La Franca, M.; Faddetta, T.; Gallo, G.; Schillaci, D.; Collina, S.; Leonchiks, A.; Barone, G. Pyrrolomycins as antimicrobial agents. Microwave-assisted organic synthesis and insights into their antimicrobial mechanism of action. *Bioorganic & medicinal chemistry* **2019**, *27*, 721–728.

(11) Raimondi, M. V.; Presentato, A.; Li Petri, G.; Buttacavoli, M.; Ribaudo, A.; De Caro, V.; Alduina, R.; Cancemi, P. New synthetic nitro-pyrrolomycins as promising antibacterial and anticancer agents. *Antibiotics* **2020**, *9*, 292.

(12) Sarg, M.; Koraa, M.; Bayoumi, A.; Abd El Gilil, S., et al. Synthesis of pyrroles and condensed pyrroles as anti-inflammatory agents with multiple activities and their molecular docking study. *Open Journal of Medicinal Chemistry* **2015**, *5*, 49.

(13) Ahmad, S.; Alam, O.; Naim, M. J.; Shaquiquzzaman, M.; Alam, M. M.; Iqbal, M. Pyrrole: An insight into recent pharmacological advances with structure activity relationship. *European journal of medicinal chemistry* **2018**, *157*, 527–561.

(14) Indumathi, S.; Karthikeyan, R.; Nasser, A. J. A.; Idhayadhulla, A.; Kumar, R. S. Anticonvulsant, analgesic and anti-inflammatory activities of some novel pyrrole and 1, 4-dihydropyridine derivatives. *J. Chem. Pharm. Res* **2015**, *7*, 434–40.

(15) Gholap, S. S. Pyrrole: An emerging scaffold for construction of valuable therapeutic agents. *European journal of medicinal chemistry* **2016**, *110*, 13–31.

(16) Nicolai, A.; Madia, V. N.; Messore, A.; De Vita, D.; De Leo, A.; Ialongo, D.; Tudino, V.; Tortorella, E.; Scipione, L.; Taurone, S., et al. Anti-Tumoral effects of a (1H-Pyrrol-1-yl) methyl-1H-Benzoimidazole carbamate Ester derivative on head and neck squamous carcinoma cell lines. *Pharmaceuticals* **2021**, *14*, 564.

(17) Zheng, L.; Gao, T.; Ge, Z.; Ma, Z.; Xu, J.; Ding, W.; Shen, L. Design, synthesis and structure-activity relationship studies of glycosylated derivatives of marine natural product Lamellarin D. *European Journal of Medicinal Chemistry* **2021**, *214*, 113226.

(18) Motati, D. R.; Uredi, D.; Watkins, E. B. The discovery and development of oxalamide and pyrrole small molecule inhibitors of gp120 and HIV entry-A review. *Current Topics in Medicinal Chemistry* **2019**, *19*, 1650–1675.

(19) Qiu, J.; Liang, T.; Wu, J.; Yu, F.; He, X.; Tian, Y.; Xie, L.; Jiang, S.; Liu, S.; Li, L. N-substituted pyrrole derivative 12m inhibits HIV-1 entry by targeting Gp41 of HIV-1 envelope glycoprotein. *Frontiers in Pharmacology* **2019**, *10*, 859.

(20) Zarganes-Tzitzikas, T.; Neochoritis, C. G.; Dömling, A. Atorvastatin (lipitor) by MCR. *ACS medicinal chemistry letters* **2019**, *10*, 389–392.

(21) Kakaawla, T. K.; Hartley, W. C.; Harrity, J. P. Synthesis and Cycloaddition Reactions of Stabilized Münchnones. *European Journal of Organic Chemistry* **2016**, *2016*, 2789–2792.

(22) Jackiewicz, V.; Arndtsen, B. A. Thieme Chemistry Journals Awardees–Where Are They Now? Phospha-Münchnone 1, 3-Dipolar Cycloaddition with Alkenes: A One-Pot Approach to 2-Pyrrolines from Imines, Acid Chlorides and Alkenes. *Synlett* **2017**, *28*, 433–438.

(23) Kolb, H. C.; Finn, M. G.; Sharpless, K. B. Click Chemistry: Diverse Chemical Function from a Few Good Reactions. *Angewandte Chemie International Edition* **2001**, *40*, 2004–2021.

(24) Devaraj, N. K.; Finn, M. G. Introduction: Click Chemistry. *Chemical Reviews* **2021**, *121*, 6697–6698, PMID: 34157843.

(25) Avalos, M.; Babiano, R.; Cabanillas, A.; Cintas, P.; Jiménez, J. L.; Palacios, J. C.; Aguilar, M. A.; Corchado, J. C.; Espinosa-García, J. Münchnone-Alkene Cycloadditions: Deviations from the FMO Theory. Theoretical Studies in the Search of the Transition State. *The Journal of Organic Chemistry* **1996**, *61*, 7291–7297, PMID: 11667652.

(26) Aly, S.; Romashko, M.; Arndtsen, B. A. Multicomponent Synthesis of Substituted and Fused-Ring Imidazoles via Phospha-münchnone Cycloaddition. *The Journal of Organic Chemistry* **2015**, *80*, 2709–2714, PMID: 25688846.

(27) Snieckus, V.; Dowling, M. Modular Assembly of Imidazoles by 1, 3-Dipolar Cycloaddition. *Synfacts* **2015**, *11*, 0469–0469.

(28) Reissig, H.-U.; Zimmer, R. Münchnones—New Facets after 50 Years. *Angewandte Chemie International Edition* **2014**, *53*, 9708–9710.

(29) Morin, M. S.; St-Cyr, D. J.; Arndtsen, B. A.; Krenske, E. H.; Houk, K. Modular mesoionics: understanding and controlling regioselectivity in 1, 3-dipolar cycloadditions of münchnone derivatives. *Journal of the American Chemical Society* **2013**, *135*, 17349–17358.

(30) St-Cyr, D. J.; Morin, M. S.; Belanger-Gariepy, F.; Arndtsen, B. A.; Krenske, E. H.; Houk, K. Phospha-Munchnones: electronic structures and 1, 3-dipolar cycloadditions. *The Journal of Organic Chemistry* **2010**, *75*, 4261–4273.

(31) Champagne, P. A.; Houk, K. Influence of endo-and exocyclic heteroatoms on stabilities and 1, 3-dipolar cycloaddition reactivities of mesoionic azomethine ylides and imines. *The Journal of organic chemistry* **2017**, *82*, 10980–10988.

(32) Lopchuk, J. M.; Hughes, R. P.; Gribble, G. W. What Controls Regiochemistry in 1, 3-Dipolar Cycloadditions of Munchnones with Nitrostyrenes? *Organic letters* **2013**, *15*, 5218–5221.

(33) Martínez González, M.; Hernández-Castillo, D.; Montero-Cabrera, L. A.; Miranda-Quintana, R. A. Geometrical distortions and charge transfer in munchnöne regioselectivity: A conceptual density functional study. *International Journal of Quantum Chemistry* **2017**, *117*, e25444.

(34) Miranda-Quintana, R. A. *Conceptual Density Functional Theory and Its Application in the Chemical Domain*; Apple Academic Press, 2018; pp 15–44.

(35) Weinhold, F. Chemical bonding as a superposition phenomenon. *Journal of chemical education* **1999**, *76*, 1141.

(36) Glendening, E. D.; Weinhold, F. Pauling's Conceptions of Hybridization and Resonance in Modern Quantum Chemistry. *Molecules* **2021**, *26*, 4110.

(37) Landis, C. R.; Weinhold, F. The NBO view of chemical bonding. *The Chemical Bond: Fundamental Aspects of Chemical Bonding* **2014**, 91–120.

(38) Amore-Bonapasta, A.; Battistoni, C.; Lapiccirella, A.; Paparazzo, E. A theoretical study of the conformational behaviour of the S-methyl ester of dithiocarbazic acid. *Journal of Molecular Structure: THEOCHEM* **1982**, *90*, 1–6.

(39) Johnson, E.; Keinan, S.; Mori-Sanchez, P.; Contreras-Garcia, J.; Cohen, A.; Yang, W. Density-functional theory, self-directed growth, electron-density, topological analysis, correlation-energy, proteins, localization, exchange, accurate, bonds. *J Am Chem Soc* **2010**, *132*, 6498–6506.

(40) De Proft, F. *Conceptual Density Functional Theory*; John Wiley & Sons, Ltd, 2022; Chapter 2, pp 17–46.

(41) Miranda-Quintana, R. A. Condensed-to-atoms hardness kernel from the response of molecular fragment approach. *Chemical Physics Letters* **2016**, *658*, 328–330.

(42) Tognetti, V.; Morell, C.; Joubert, L. Quantifying electro/nucleophilicity by partitioning the dual descriptor. *Journal of Computational Chemistry* **2015**, *36*, 649–659.

(43) Reed, A. E.; Weinstock, R. B.; Weinhold, F. Natural population analysis. *The Journal of Chemical Physics* **1985**, *83*, 735–746.

(44) Tsirelson, V. G.; Stash, A. I.; Liu, S. Quantifying steric effect with experimental electron density. *The Journal of chemical physics* **2010**, *133*, 114110.

(45) Liu, S.; Liu, L.; Yu, D.; Rong, C.; Lu, T. Steric charge. *Physical Chemistry Chemical Physics* **2018**, *20*, 1408–1420.

(46) Liu, S. Origin and Nature of Bond Rotation Barriers: A Unified View. *The Journal of Physical Chemistry A* **2013**, *117*, 962–965.

(47) Liu, S.; Hu, H.; Pedersen, L. G. Steric, Quantum, and Electrostatic Effects on S_N2 Reaction Barriers in Gas Phase. *The Journal of Physical Chemistry A* **2010**, *114*, 5913–5918.

(48) Liu, S. Steric effect: A quantitative description from density functional theory. *The Journal of Chemical Physics* **2007**, *126*, 244103.

(49) Miranda-Quintana, R. A.; Ayers, P. W. Interpolation of property-values between electron numbers is inconsistent with ensemble averaging. *The Journal of Chemical Physics* **2016**, *144*, 244112.

(50) Johnson, P. A.; Bartolotti, L. J.; Ayers, P. W.; Fievez, T.; Geerlings, P. In *Modern Charge-Density Analysis*; Gatti, C., Macchi, P., Eds.; Springer Netherlands: Dordrecht, 2012; pp 715–764.

(51) Gázquez, J. Chemical reactivity concepts in density functional theory. *Chemical reactivity theory: a density functional view* **2009**, 7–21.

(52) Miranda-Quintana, A. R., and Ayers, PW (2016a). Charge Transfer and Chemical Potential in 1, 3-dipolar Cycloadditions. *Theor. Chem. Accounts 135*.

(53) Miranda-Quintana, R. A.; Ayers, P. W. Charge transfer and chemical potential in 1,3-dipolar cycloadditions. *Theoretical Chemistry Accounts* **2016**, *135*, 172.

(54) Miranda-Quintana, R. A. Perturbed reactivity descriptors: the chemical hardness. *Theoretical Chemistry Accounts* **2017**, *136*, 1–8.

(55) Geerlings, P.; Proft, F. D.; Langenaeker, W. Conceptual Density Functional Theory. *Chemical Reviews* **2003**, *103*, 1793–1874.

(56) Miranda-Quintana, R. A. Thermodynamic electrophilicity. *The Journal of Chemical Physics* **2017**, *146*, 214113.

(57) Parr, R. G.; v. Szentpály, L.; Liu, S. Electrophilicity Index. *Journal of the American Chemical Society* **1999**, *121*, 1922–1924.

(58) Chamorro, E.; Chattaraj, P. K.; Fuentealba, P. Variation of the Electrophilicity Index along the Reaction Path. *The Journal of Physical Chemistry A* **2003**, *107*, 7068–7072.

(59) Miranda-Quintana, R. A.; Ayers, P. W. Dipolar cycloadditions and the "$|\Delta\mu|$ big is good" rule: a computational study. *Theoretical Chemistry Accounts* **2018**, *137*, 1–7.

(60) Miranda-Quintana, R. A.; Heidar-Zadeh, F.; Ayers, P. W. Elementary derivation of the "$|\Delta\mu|$ big is good" rule. *The Journal of Physical Chemistry Letters* **2018**, *9*, 4344–4348.

(61) Miranda-Quintana, R. A.; Ayers, P. W.; Heidar-Zadeh, F. Reactivity and Charge Transfer Beyond the Parabolic Model: the "$|\Delta\mu|$ Big is Good" Principle. *ChemistrySelect* **2021**, *6*, 96–100.

(62) Miranda-Quintana, R. A.; Ayers, P. W. Note: Maximum hardness and minimum electrophilicity principles. *The Journal of Chemical Physics* **2018**, *148*, 196101.

(63) Pearson, R. G. Hard and soft acids and bases, HSAB, part 1: Fundamental principles. *Journal of Chemical Education* **1968**, *45*, 581.

(64) Martínez González, M.; Cárdenas, C.; Rodríguez, J. I.; Liu, S.; Heidar-Zadeh, F.; Miranda-quintana, R. A.; Ayers, P. W. Quantitative electrophilicity measures. *Acta Phys. -Chim. Sin.* **2018**, *34*, 662–674.

(65) Miranda-Quintana, R. A.; Chattaraj, P. K.; Ayers, P. W. Finite temperature grand canonical ensemble study of the minimum electrophilicity principle. *The Journal of Chemical Physics* **2017**, *147*, 124103.

(66) Heidar-Zadeh, F.; Miranda-Quintana, R. A.; Verstraelen, T.; Bultinck, P.; Ayers, P. W. When is the Fukui function not normalized? The danger of inconsistent energy interpolation models in density functional theory. *Journal of Chemical Theory and Computation* **2016**, *12*, 5777–5787.

(67) Yang, W.; Parr, R. G.; Pucci, R. Electron density, Kohn–Sham frontier orbitals, and Fukui functions. *The Journal of Chemical Physics* **1984**, *81*, 2862–2863.

(68) Wang, B.; Rong, C.; Chattaraj, P. K.; Liu, S. A comparative study to predict regioselectivity, electrophilicity and nucleophilicity with Fukui function and Hirshfeld charge. *Theoretical Chemistry Accounts* **2019**, *138*.

(69) Zamora, P.; Bieger, K.; Cuchillo, A.; Tello, A.; Muena, J. Theoretical determination of a reaction intermediate: Fukui function analysis, dual reactivity descriptor and activation energy. *Journal of Molecular Structure* **2021**, *1227*, 129369.

(70) Morell, C.; Grand, A.; Toro-Labbé, A. New Dual Descriptor for Chemical Reactivity. *The Journal of Physical Chemistry A* **2004**, *109*, 205–212.

(71) Miranda-Quintana, R. A.; González, M. M.; Hernández-Castillo, D.; Montero-Cabrera, L. A.; Ayers, P. W.; Morell, C. Conceptual DFT analysis of the regioselectivity of 1, 3-dipolar cycloadditions: nitrones as a case of study. *Journal of Molecular Modeling* **2017**, *23*, 1–15.

(72) Vidhya, V.; Austine, A.; Arivazhagan, M. Molecular structure, aromaticity, vibrational investigation and dual descriptor for chemical reactivity on 1- chloroisoquinoline using quantum chemical studies. *Results in Materials* **2020**, *6*, 100097.

(73) Frau, J.; Glossman-Mitnik, D. Conceptual DFT study of the local chemical reactivity of the dilysyldipyrrolones A and B intermediate melanoidins. *Theoretical Chemistry Accounts* **2018**, *137*.

(74) Miranda-Quintana, R. A.; Bochicchio, R. C. Energy dependence with the number of particles: density and reduced density matrices functionals. *Chemical Physics Letters* **2014**, *593*, 35–39.

(75) Miranda-Quintana, R. A.; Rial, D. Communication: Reduced density matrices in molecular systems: Grand-canonical electron states. *Journal of Chemical Physics* **2013**, *139*.

(76) Miranda-Quintana, R. A.; Ayers, P. W. Fractional electron number, temperature, and perturbations in chemical reactions. *Phys. Chem. Chem. Phys.* **2016**, *18*, 15070–15080.

(77) Galván, M.; Gázquez, J. L.; Vela, A. Fukui function: Spin-density and chemical reactivity. *The Journal of Chemical Physics* **1986**, *85*, 2337–2338.

(78) Pearson, R. G. Hard and Soft Acids and Bases. *Journal of the American Chemical Society* **1963**, *85*, 3533–3539.

(79) Mendez, F.; Gazquez, J. L. Chemical Reactivity of Enolate Ions: The Local Hard and Soft Acids and Bases Principle Viewpoint. *Journal of the American Chemical Society* **1994**, *116*, 9298–9301.

(80) Langenaeker, W.; de Proft, F.; Geerlings, P. Development of Local Hardness-Related Reactivity Indices: Their Application in a Study of the SE at Monosubstituted Benzenes within the HSAB Context. *The Journal of Physical Chemistry* **1995**, *99*, 6424–6431.

(81) Geerlings, P.; Proft, F. D. HSAB principle: Applications of its global and local forms in organic chemistry. *International Journal of Quantum Chemistry* **2000**, *80*, 227–235.

(82) Frisch, M. J. et al. Gaussian-09 Revision E.01. Gaussian Inc. Wallingford CT 2009.

(83) Bickelhaupt, F. M.; Houk, K. N. Analyzing Reaction Rates with the Distortion/Interaction-Activation Strain Model. *Angewandte Chemie International Edition* **2017**, *56*, 10070–10086.

(84) Lu, T.; Chen, F. Multiwfn: A multifunctional wavefunction analyzer. *Journal of Computational Chemistry* **2012**, *33*, 580–592.

(85) Reed, A. E.; Curtiss, L. A.; Weinhold, F. Intermolecular interactions from a natural bond orbital, donor-acceptor viewpoint. *Chemical Reviews* **1988**, *88*, 899–926.

(86) Sjoberg, P.; Murray, J. S.; Brinck, T.; Politzer, P. Average local ionization energies on the molecular surfaces of aromatic systems as guides to chemical reactivity. *Canadian Journal of Chemistry* **1990**, *68*, 1440–1443.

(87) Politzer, P.; Murray, J. S.; Bulat, F. A. Average local ionization energy: A review. *Journal of Molecular Modeling* **2010**, *16*, 1731–1742.

TOC Graphic

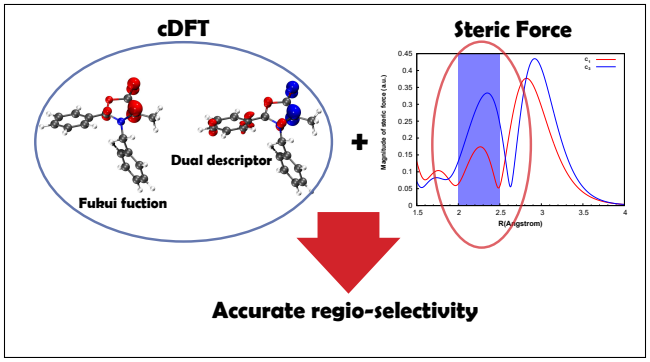
cDFT
Steric Force
Dual descriptor
Fukui fuction
Accurate regio-selectivity